Desalination and Water Treatment
www.deswater.com
doi: 10.5004/dwt.2022.28649

267 (2022) 201–214
August

Removal of malachite green using ultrasound-assisted and conventional batch adsorption based on *Paracentrotus lividus* shells as biosorbent

Chawki Djelloul[a,*], Houria Ghodbane[b,c]

[a]*Laboratory of Reaction Engineering, Faculty of Mechanical Engineering and Process Engineering, USTHB, Algiers, Algeria, email: djelloulchawki@yahoo.fr*
[b]*Faculty of Science and Technology, Department of Process Engineering,, University of Souk Ahras, Souk Ahras, Algeria, email: hiba_ghodbane@yahoo.fr*
[c]*Laboratory of Physics of Matter and Radiation, Mohamed Cherif Messadia-Souk Ahras University, P.O. Box: 1553, Souk Ahras 41000, Algeria*

Received 12 January 2022; Accepted 10 June 2022

ABSTRACT

The purpose of this investigation is the evaluation of the *Paracentrotus lividus* shells (PLS) as a new inexpensive non-conventional biosorbent for the removal of malachite green (MG) from water by mechanical agitation or ultrasonic irradiation under various operating conditions in a batch process. The PLS have been characterized by scanning electron microscope and Fourier-transform infrared spectrometer. The findings revealed that the adsorption rate of MG was improved when ultrasound was used; equilibrium time is reduced in half when using ultrasound instead mechanical stirring. The influence of operating conditions such as initial dye concentration (2–10 mg/L), adsorbent dose (0.2–0.8 g), particle size (850–2,000 μm), stirring speed (0–200 rpm), temperature (21°C–50°C), ionic strength (0–5 g/L) and initial solution pH (2–9) on the removal of MG was investigated. Basic pH conditions are more propitious for the adsorption of MG. The equilibrium time decreases from 420 to 60 min when the temperature increases from 21°C to 50°C. Biosorption kinetics obtained at different biosorbent doses were analyzed using Lagergren pseudo-first-order, Blanchard pseudo-second-order, Elovich and intraparticle diffusion models. The kinetic data are excellently fitted by the pseudo-second-order kinetics model for the stirring method and sonication method. For adsorption by stirring, experimental equilibrium data were best represented by Temkin model followed by form 1 of the Langmuir model followed by the Freundlich model. Additionally, the adsorption by sonication is better described by the Harkins–Jura model followed by form 2 of the Langmuir model and the Freundlich model. The results in this study indicated that PLS was an attractive candidate for removing cationic dyes from the dye wastewater and the use of ultrasonic radiation instead of mechanical agitation seems to be a very interesting technique to speed up the biosorption process.

Keywords: Sono-sorption; Malachite green; *Paracentrotus lividus* shells; Kinetics; Isotherm; Modeling

1. Introduction

The availability of sufficient quantity and good quality of water is a major challenge faced nowadays all over the world and it is utmost important to protect this scarce good from the pollution that can be caused by different pollutants. Dyes are one of the major pollutants found in industrial effluents and causing significant water pollution [1].

The use of dyes in water prevents sunlight penetration into aquatic plants, leads to toxicity in water owing to the

* Corresponding author.

degraded products and also raises the chemical oxygen demand of water masses [2]. Synthetic origin and complex structure of dyes are making them non-biodegradable, stable and hence it is difficult to treat dye-containing wastewater [3]. Dye bearing wastewater treatment is of 64 primary concern as even at very low concentrations, dyes decrease water clarity and hence are undesirable [4].

Therefore, the removal of these relevant chemical compounds from industrial effluents and wastewater is necessary via the application of a reliable technology [5–12]. Indeed, the adsorption is an effective removal process that has been largely applied for water decolorization in comparison to other treatment techniques like flocculation, membrane separation and chemical oxidation [13]. The advantages of adsorption include its simple design, regeneration capability and excellent separation performance [14–16].

In recent years different biosorbent material has been used in attempts to remove organic material and color. Though effective color removal may be obtained with active carbon, it is very expensive [17].

The use of inexpensive, efficient and naturally abundant materials involving reduced treatment like agricultural by-products from agriculture and the food industry have been commonly applied as biosorbents for the disposal of dyes recently [18]. Shells were already utilized as a new inexpensive non-conventional biosorbent for the removal of pollutants from the aqueous phase [19,20]. Given that marine biosorbents are currently available and may be used to remove pollutants from the water environment, *Paracentrotus lividus* shells (PLS) have been chosen as an appropriate material for water treatment.

Ultrasonic waves are wildly used in metallurgy, modification and chemical industries due to the advantage of mechanical action and acoustic cavitation [17].

In order to improve the efficiency of the adsorption of various pollutants from aqueous solutions, the use of ultrasound has been examined lately and some controversial results have been published. Li et al. [21] have indicated that the adsorptive capacity of activated carbon for phenol is decreased when ultrasound is used. A number of investigations have mentioned the beneficial impact of ultrasound on the adsorption process via the enhancement of mass transfer rate in solid–liquid systems [22–26].

The present article is novel in terms of effective utilization of PLS as an inexpensive biosorbent with significant uptake of targeted dye in batch studies. Moreover, no specific study has been done on the biosorption of malachite green (MG), as a representative of cationic dyes, onto PLS in the presence of low frequency ultrasound. In this regard, the aim of the present study is to characterize the untreated PLS in order to study the efficiency of biomaterial chosen for the removal of malachite green dye from aqueous solutions in the absence (stirring) and presence of low frequency ultrasound (no stirring). Biosorption parameters including the dye concentration in the solution, the contact time with biosorbent, the dose of biosorbent, ionic strength and particle size were investigated to study the biosorption efficiency by both methods. Biosorption mechanisms were then suggested by the study of the isotherms and kinetics of biosorption.

2. Materials and methods

2.1. Sorbate preparation

Malachite green (characteristics given in Table 1) was purchased from Biochem (Chemopharma, France) and was used as sorbate. A stock solution of malachite green (1 g/L) was prepared in distilled water and was used for the adsorption study. In order to adjust the pH solutions, 0.10 mol/L sodium hydroxide or hydrochloric acid solutions were used, and the measurements were made by using a pH/meter NAHITA 903 provided with combined glass electrode.

2.2. Preparation of biosorbent

Paracentrotus lividus were collected from the Mediterranean Sea Saint Cloud, Algeria. The PLS are removed as a waste. The material chosen were firstly washed with boiled and distilled water for several times, and then dried in an oven (Binder) at 50°C for 4 d to remove moisture content. The dried material was then crushed and sieved to obtain a particle size range of 0.850–2 mm. The obtained material was washed repeatedly with distilled water until the wash water contained no color. Finally, the resulting material was subsequently dried in an oven at 50°C for 5 d to a constant weight and preserved in a desiccator prior to use.

2.3. Characterization of biosorbent

In the case of PLS, Fourier-transform infrared analysis (FTIR-8400S) has been undertaken to identify the surface functional groups, where spectra between 4,000 and 400 cm^{-1} have been obtained.

Scanning electron microscopy (SEM) images of the PLS both before and after biosorption of malachite green with and without ultrasound were captured via Quanta FEG scanning electron microscopy equipment (FEI, Oregon, USA).

An EDAX (EDAX TEAM EDS system) integrated with the SEM was used to evaluate the composition of the selected biomaterial.

Table 1
Chemical properties and characteristics of malachite green

Generic name	Malachite green
Chemical formula	$C_{52}H_{56}N_4O_{12}$
Molecular weight (g/mol)	927.02
Type of dye	Cationic
λ_{max} (nm)	617
Chemical structure	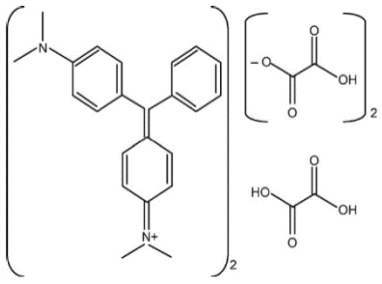

2.4. Experimental setup

A schematic diagram of the experimental setup is shown in Fig. 1. A 400 mL cylindrical glass vessel was employed for the experiments. The container was placed in an ultrasonic cleaning bath functioning at a frequency of 45 kHz with an electric power rating of 120 W. The temperature of the suspension was controlled at 21°C ± 1°C. The temperature inside the ultrasonic bath was monitored using a thermocouple immersed in the medium. Acoustic power dissipated in the medium was measured using standard calorimetric method [27]. For all the experiments, the MG solution volume treated was 100 mL.

2.5. Procedures

The experimental sets were planned on the basis of variation in various parameters such as biosorbent dosage, initial concentration of the pollutant, pH, ionic strength and particle size. The results of the experiments were compared with the biosorption in conventional conditions (i.e., the control case) to assess the enhancement effect of ultrasound. For the determination of dye removing kinetics, a preselected mass of PLS was brought into direct connection with 100 mL of MG solutions. At a fixed shaking speed of 200 rpm (the usual method), the system was agitated. All experiments were carried out with natural solution pH (4.0) with a particle size of the adsorbent of 0.85 mm except when studying the effect of the particle size where it varies from 0.85 to 2 mm.

The final concentration of MG was evaluated at selected time intervals according to a UV-Vis spectrophotometer (SECOMAM, Model UVILINE 94000) calibrated at a wavelength of 617 nm.

The dye removal efficiency, R (%), was defined by the relationship:

$$R(\%) = \left(\frac{C_0 - C_e}{C_0}\right) \times 100 \quad (1)$$

However, the biosorbed dye amount at time t, q_t (mg/g), and the equilibrium biosorption ability, q_e (mg/g), have been estimated by the following equations accordingly:

$$q_t = \left(\frac{C_0 - C_t}{m}\right) V \quad (2)$$

$$q_e = \left(\frac{C_0 - C_e}{m}\right) V \quad (3)$$

where C_0, C_e and C_t (mg/L) are the dye concentrations initially, at equilibrium and at time t, respectively, V (L) is the volume of the dye solution and m (g) is the mass of the biosorbent. All experiments were carried out in duplicate and the dye concentration of each sample was regarded equal to the mean value of the two measurements.

Equilibrium isotherms were determined by contacting a fixed mass of biosorbent (0.4 g) with 100 mL of MG solutions at 21°C ± 1°C. The mixture was then agitated at a constant speed of 200 rpm or sonicated.

Pseudo-first-order, pseudo-second-order, Elovich and intraparticle diffusion models were investigated for the experimental data fitting in order to establish the kinetic mechanism of the biosorption process in the absence and presence of ultrasound. Intraparticle and film diffusion models were applied to assess the kinetic controlling step in the studied biosorption and sono-biosorption systems.

2.6. Analysis

A well-known procedure for determining MG concentrations, based on Beer's law calibration plots, was applied using a UV–Visible spectrophotometer (SECOMAM, Model UVILINE 94000). The wavelength resolution and the bandwidth were, respectively, 1 and 0.5 nm. The length of the optical path in glass cell was 1 cm. The maximum absorption wavelength was determined as equal to 617 nm.

3. Results and discussion

3.1. Characterization of the adsorbent

3.1.2. Fourier-transform infrared spectroscopy

A graphically illustrated FTIR spectrum of PLS is depicted in Fig. 2. Based on this figure, a detection of the peak at 3,711 cm^{-1}, attributed to the stretching vibrations

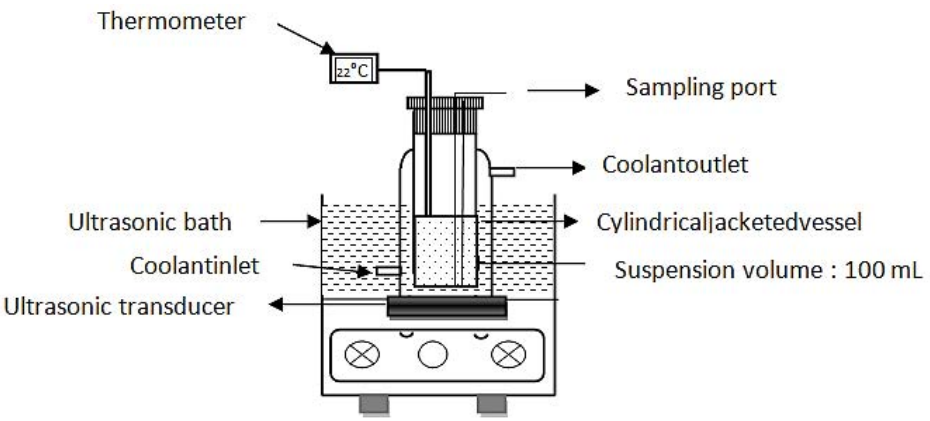

Fig. 1. Experimental set-up.

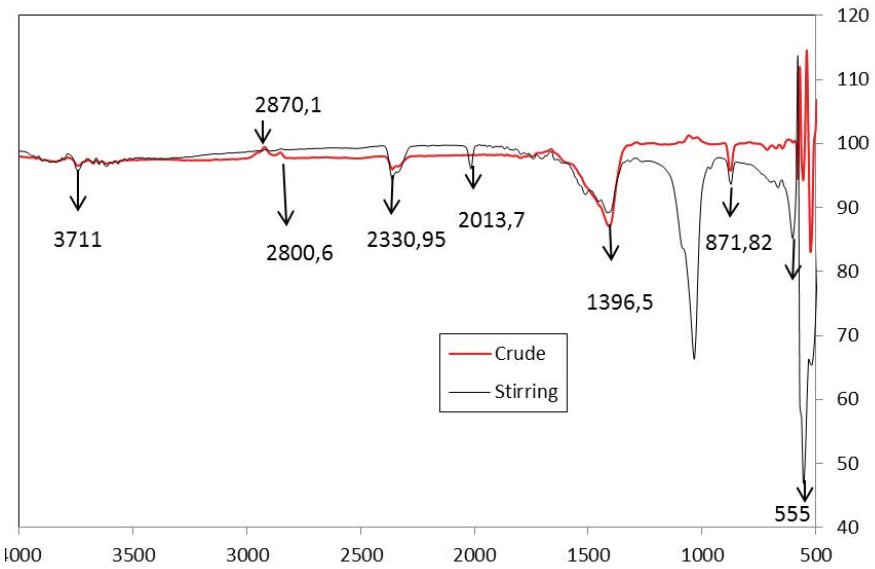

Fig. 2. FTIR spectra of PLS (*Paracentrotus lividus* shells) before and after dye biosorption.

linked to the hydroxyl OH or amine N–H groups, can be seen by superimposing the two infrared spectra, that of our adsorbent before and after treatment. A small intensification of the peak at 2,330 cm^{-1} relative to the raw peak and the occurrence of a low intensity peak at 2,013 cm^{-1} were also detected, the fact that these two peaks are found in this region of the spectrum possibly corresponds to the presence of the nitrile or alkyne function. An intense peak at 1,033 cm^{-1} was attributed to elongation vibrations, which clearly indicates the presence of the C–O or C–N bond, which may support the association of the peak at 3,711 cm^{-1}.

In the area between 601 and 524 cm^{-1}, it could notice the appearance of several bands of about equal intensity, while on the spectrum of our adsorbent and after treatment with the pollutant we noticed the presence of two new peaks at 601 and 515 cm^{-1}, which indicates without any doubt the presence of aromatic ring.

The SEM technique was employed to observe the surface physical morphology of the PLS before (Fig. 3a and b) and after adsorption of malachite green in the absence (Fig. 3c) and presence (Fig. 3d) of ultrasound. The PLS exhibits a rough surface with heterogeneous pores and cavities which enhanced the adsorption of MG dye. In addition, samples of biosorbed dye appear to have very clear dark spots in the SEM images, which can be interpreted as a sign of effective biosorption of the dye molecules into the cavities and pores of the sorbent.

SEM characterization of PLS, before and after adsorption, showed a complete change in surface texture. Before adsorption, there was a rough surface morphology as observed, while after adsorption of dye on the PLS, layer on the surface of the adsorbent and smoother morphology was observed (Fig. 3c).

The surface became rough with a new porous structure created in the presence of ultrasound as shown in Fig. 3d. The formation of the porous structure is due to the hydrodynamic cavitation effect of ultrasound.

3.2. Effect of contact time

Prior to carrying out the adsorption experiments, it was examined what effect ultrasound has on the degradation of MG. In our conditions (40 kHz, 9 W of acoustic power dissipated in the medium, and MG concentrations 2–10 mg/L), the obtained results (data not shown) demonstrate that MG degradation was not noticeable until a sonication time of 5 h.

Discontinuous experiments have been performed to examine the elimination of MG by biosorption and sono-biosorption. Initial dye concentration, biosorbent dosage and contact time were set to 10 mg/L, 0.4 g/100 mL and 180 min, respectively.

The kinetic findings of MG biosorption by PLS both in the absence (conventional method by simple mechanical agitation) and in the presence of ultrasound are shown in Fig. 4. Based on this figure, there are unique, smooth and continuous contact time plots towards equilibrium, pointing to the eventual monolayer coverage of the dye on the surface of PLS.

Both methods seem to have the seam speed in the beginning until 20 min, but from this time, the sono-sorption becomes faster. One reason for this may be the existence of shallow sites that are easily occupied by the pollutant at the beginning.

After saturation of the superficial sites, the adsorption, by mechanical stirring, on sites deep in the pores becomes more and more difficult. On the other hand, ultrasound can accelerate the migration of pollutants into the pores.

Apart from this, the adsorbent surface porosity and mass transfer rate across the liquid–solid interfaces are enhanced by ultrasonic irradiation by way of physical phenomena involving acoustic waves, microscopic turbulence, microscopic flow, high velocity micro-jets and high shear force while cavitation bubbles collapse [28–31]. This pulls the dye molecules through the porous structure of

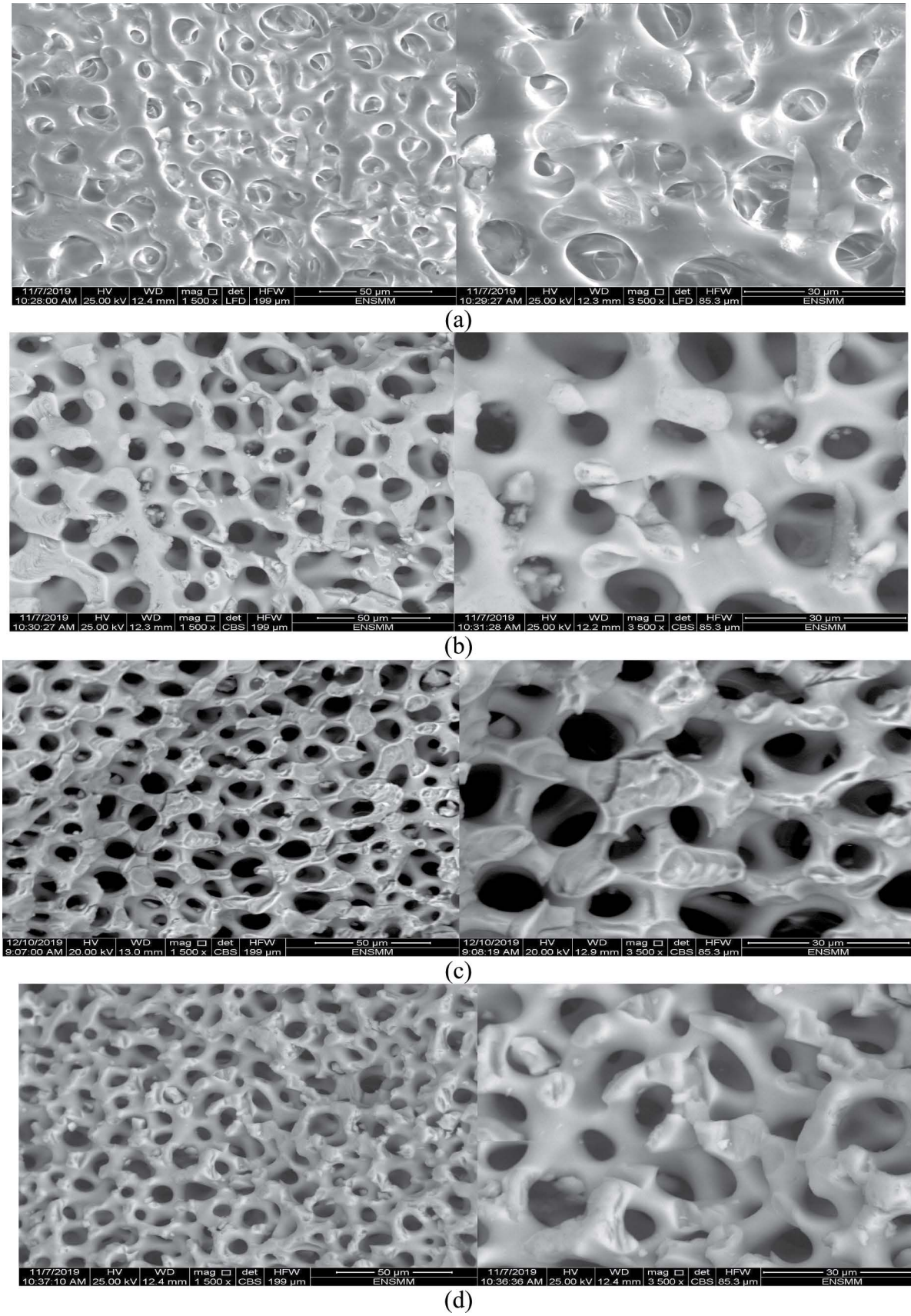

Fig. 3. SEM micrograph of *Paracentrotus lividus* shells before (a, b) and after MG biosorption by stirring (c) and by sonication (d).

the crude biosorbent, causing more active biosorbent sites. Alternatively, ultrasonication can be conducted to achieve a homogeneous pattern of active adsorbent sites in the adsorbent for efficient dye molecule trapping [30,32].

3.3. Effect of adsorbent's dose

The adsorption of malachite green at the surface of *Paracentrotus lividus* shell was studied using the conventional method and sonication alone by changing the quantity of adsorbent (0.2–0.8 g/100 mL) in the test solution, while keeping at constant values the initial dye concentration at 10 mg/L, the temperature at 21°C ± 1°C, and the contact time for 180 min. The increase in the percentage of removal is no longer significant when the sorbent concentration exceeds 0.4 g/100 mL (figure not shown). The impact of the biosorbent dose on the extent of MG biosorbed for the conventional method and sonication is plotted in Fig. 5. The quantity of MG biosorbed dropped in all cases as the dose of biosorbent was raised. The quantity adsorbed by 0.2 g of adsorbent with stirring represents less than three quarters of the quantity adsorbed by the same dose of adsorbent with ultrasound. The higher mass transfer in the presence of ultrasonic irradiation seems to be a probable reason for this. This improvement may be explained by the intensification of mass transfer phenomena through acoustic vortex microstreaming, shockwaves, microjets, and thermal effects of ultrasound. With the highest biosorbent dose, there was little increase in biosorption in the presence of ultrasound, reflecting the greater accessibility of the biosorption sites. Analogous results have been published in the literature [33,34].

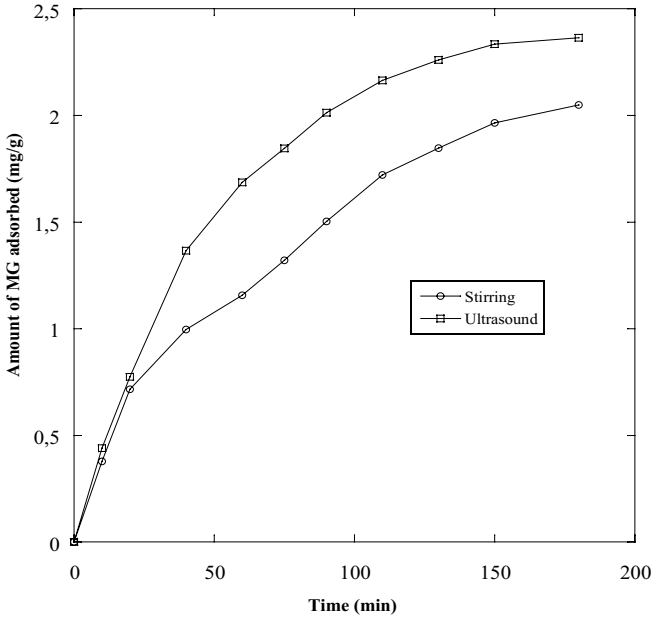

Fig. 4. Biosorption of malachite green by PLS in the absence and presence of ultrasound (T = 21°C; biosorbent dose = 0.4 g/100 mL; initial concentration = 10 mg/L; stirring speed = 300 rpm or sonication power = 9 W; contact time = 180 min).

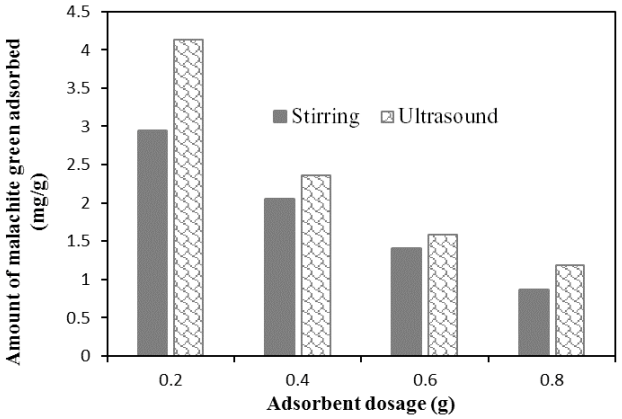

Fig. 5. Amount of malachite green biosorbed in the absence and presence of ultrasound for different adsorbent dosages (T = 21°C; biosorbent dose = 0.2–0.8 g/100 mL; initial concentration = 10 mg/L; stirring speed = 300 rpm or sonication power = 9 W; contact time = 180 min).

3.4. Effect of biosorbent particle size

The effect of particle size of *Paracentrotus lividus* shell on the dye removal was studied by varying the particle size from 0.85 mm at 2.0 mm, while keeping at constant values the initial dye concentration at 10 mg/L, the temperature at 21°C ± 1°C, and the contact time for 180 min. Fig. 6 shows minimum particle size showed greater adsorption than larger size for both methods. Increasing the biosorption surface area with the smallest particle size of the biosorbent. As particle size decreases, the increase in biosorption capacity suggests that the dye adsorbed preferentially on the outer surface and did not completely penetrate the particle due to steric hindrance of large dye molecules. As particle size decreases, the ability to adsorb increased, this is because the smaller particles have more surface area and access to the particle pores is facilitated when their size is small, implying that the dye has preferentially biosorbed on the exterior surface and has not fully penetrated the particle due to steric hindrance of large dye molecules [35].

3.5. Effect of stirring speed

For the purposes of examining the impact of shaking speed on MG biosorption, suitable experiments were undertaken at an initial dye concentration of 10 mg/L, a temperature of 21°C ± 1°C, an adsorbent dose of 0.4 g/100 mL, a biosorbent particle size of 0.85 mm and a contact time of 180 min. The agitation speed impact is given in Fig. 7, which shows that amount of MG adsorbed increases with increasing the stirring speed until 200 rpm. The effect of stirring speed seems negligible for speeds above 200 rpm. The increase of stirring speed increases the removal efficiency by decreasing the thickness of the diffusion layer around the biosorbent surface [36].

3.6. Effect of temperature

The effect of temperature to the biosorption capacity of MG was carried out at 21°C, 30°C, 40°C and 50°C at an initial dye concentration of 10 mg/L, adsorbent dose at (0.4 g/100 mL), a particle size of the adsorbent of 0.85 mm

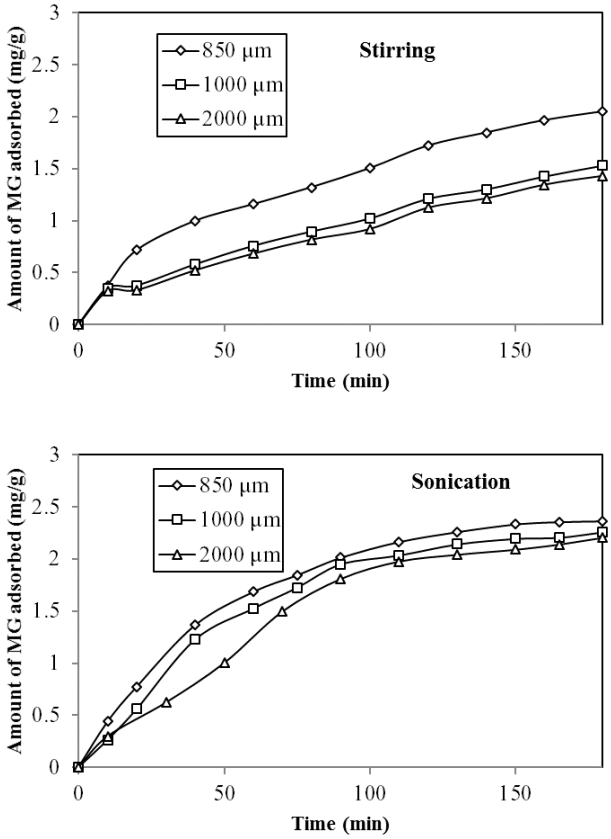

Fig. 6. Amount of malachite green biosorbed in the absence and presence of ultrasound for different particle size (T = 21°C; biosorbent dose = 0.4 g/100 mL; initial concentration = 10 mg/L; stirring speed = 300 rpm or sonication power = 9 W; contact time = 180 min).

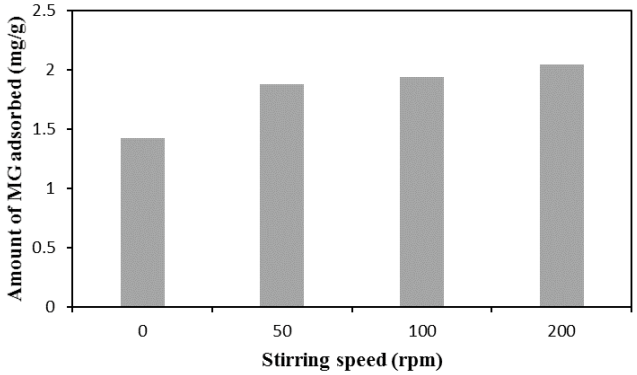

Fig. 7. Amount of malachite green biosorbed for different stirring speed (stirring speed: 0–200 rpm; T = 21°C; biosorbent dose = 0.4 g/100 mL; initial concentration = 10 mg/L; contact time = 180 min).

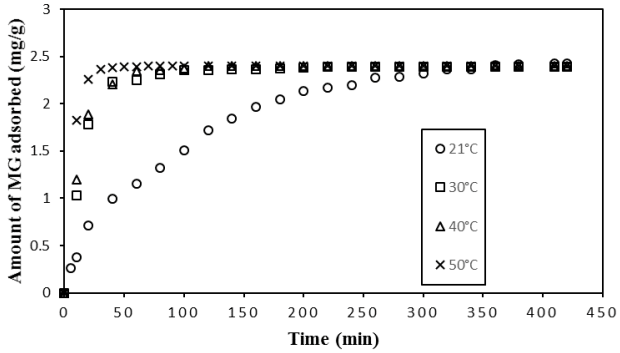

Fig. 8. Amount of malachite green biosorbed for different temperature (T = 21°C–50°C; adsorbent dose = 0.4 g/100 mL; initial concentration = 10 mg/L; stirring speed = 200 rpm).

and the contact time until equilibrium, results are shown in Fig. 8. It was observed that the equilibrium time decreases as the temperature increases. At 50°C, equilibrium is reached after 60 min of stirring, on the other hand, at 21°C; equilibrium is reached after 420 min. For kinetics, the increase in temperature accelerates the diffusion through the film and into the pores because of the decrease in the viscosity of the solution [37] but for the amount adsorbed at equilibrium; it is found that the temperature has no remarkable effect on the sorption.

It seems that the temperature has two contradictory effects on the adsorption of MG on the PLS; an adsorption-promoting effect related to the enhancement of the diffusivity of the dye through the boundary layer and into the pores, and an adsorption-disadvantaging effect related to the breaking of the weak bond between the sorbent and the sorbate (section 3.10).

The result of these two effects is that the adsorption rate increases with the increase in temperature but the quantity sorbed at equilibrium remains unchanged. Similar results were found by Cengiz and Cavas et al. [38].

3.7. Effect of ionic strength

The effect of ionic strength on the biosorption of MG on by PLS by the conventional method (stirring) was studied with a constant initial concentration of 10 mg/L, biosorbent mass of 0.4 g, temperature of 21°C ± 1°C, stirring speed of 200 rpm and different concentrations of sodium chloride (0–5 g/L) and contact time until equilibrium. The effect of inorganic salt (NaCl) on adsorption rate of MG is presented in Fig. 9. Studies showed that the adsorption decreased with increase in ionic strength; when ionic strength increases from 0 to 5 mg/L of salt, the amount adsorbed decreased from 2.43 to 2.2 mg/g. It seems that the Na^+ cations compete with the cations of the MG to occupy adsorption sites.

3.8. Effect of initial dye concentration

A study of the impact of the initial dye concentration on the extent of biosorption to the shell surface of *Paracentrotus lividus* was done by means of the conventional method and by conducting sonication alone by changing the initial concentration of malachite green in the test solution (2–10 mg/L), while keeping the dose of biosorbent at (0.4 g/100 mL), the temperature at 21°C ± 1°C, and the contact time until equilibrium constant. The results are presented in Fig. 10. For the different concentrations tested, it can be observed that the biosorption, for both methods, is rapid in the initial stages and gradually decreases with the biosorption progress until the equilibrium. Raising

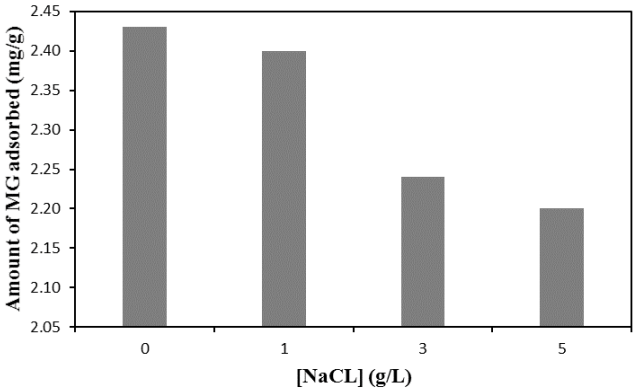

Fig. 9. Amount of malachite green biosorbed for different ionic strength ([NaCL] = 0–5 g/L; T = 21°C; adsorbent dose = 0.4 g/100 mL; initial concentration = 10 mg/L; stirring speed = 200 rpm).

the initial dye concentration will eventually result in an enhanced biosorption capacity of the MG. The equilibrium adsorption amounts are the same for both biosorption methods, but with the sonication method, equilibrium is reached after 3 h, whereas with the stirring method, equilibrium is reached after more than 6 h. Similar observations have further been obtained in the biosorption of methylene blue by Djelloul et al. [33]. Ultrasound has been shown to enhance MG elimination due to the extreme conditions created by cavitation bubbles. The use of ultrasound can raise the rate of biosorption by speeding up mass transfer based on hydrodynamic effects induced by acoustic cavitation [39].

3.9. Effect of initial solution pH

The effect of pH on the sorption of MG from aqueous solutions by PLS was observed using the conventional method and sonication alone at varying pH from 2 to 9 with 21°C temperature, 0.2 g/100 mL biosorbent concentration, 10 mg/L initial dye concentration and 210 min of contact time. It can be seen that the biosorption increases with the increase in initial pH. pH_{PZC} of PLS is equal to 8.8. The result presented in Fig. 11 shows that the sorption is better at basic pH; the higher the pH of the solution, the higher the sorption capacity and the percentage of dye removal. This can be explained by the fact that the pH of the solution governs the electrostatic forces. At low pH values (2 and 3), lower sorption capacity at equilibrium was observed, this is maybe due to the concurrency between hydronium ions and the cations of the MG. Also, the surface of the biosorbent was protonated with excessive H^+, making the sites of the biosorbent positively charged with strong electrostatic repulsion for cations [40,41].

Above pH 4, the improvement in sorption is not very significant. During the pH effect experiments, the final pH of suspensions with initial pH values of 4–8 converged rapidly (<5 min) to pH_{PZC} (8.8). At pH > pH_{ZPC}, the surface of the PLS gets negatively charged and favors uptake of cationic dye.

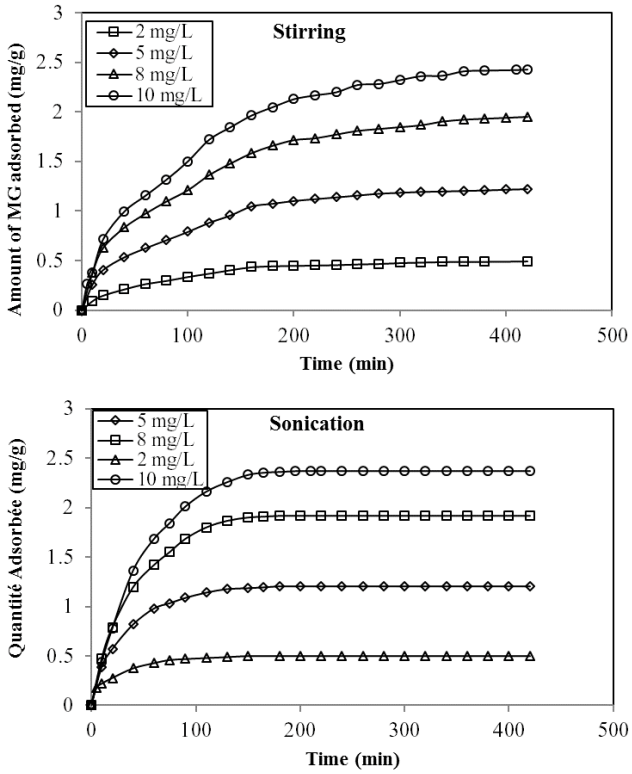

Fig. 10. Amount of malachite green biosorbed in the absence and presence of ultrasound for different initial dye concentration (T = 21°C; biosorbent dose = 0.4 g/100 mL; initial concentration = 2–10 mg/L; stirring speed = 200 rpm or sonication power = 9 W).

3.10. Modeling of biosorption kinetics and mechanism

Kinetic models were used to test the experimental data obtained by the two methods studied for different doses of biosorbent. Biosorption data was subjected to the Lagergren [42], the Blanchard [43], the Elovich [44] and the Weber and Morris [45] models. The best-fit model was selected based on the magnitude of the regression correlation coefficient (r) as a first criterion, and the experimental amount biosorbed at equilibrium (q_e) will be close to the theoretical (calculate) amount biosorbed as a second one if the model allows it to be calculated.

The kinetic data were analyzed using the Lagergren pseudo-first-order models which can be written as:

$$\ln\left(q_e - q_t\right) = k_1 t + \ln\left(q_e\right) \tag{4}$$

where q_t is the amount of biosorbate biosorbed at time t (mg/g), q_e is the biosorption capacity in the equilibrium (mg/g), k_1 is the pseudo-first-order rate constant (min^{-1}) and t is the contact time (min).

The plot of $\ln(q_e - q_t)$ vs. t gives a straight line. The slope of plot was used to determine the equilibrium rate constant, k_1, and the intercept for the biosorption at equilibrium, q_e.

Blanchard pseudo-second-order kinetic model expressed by the following linearized form [46].

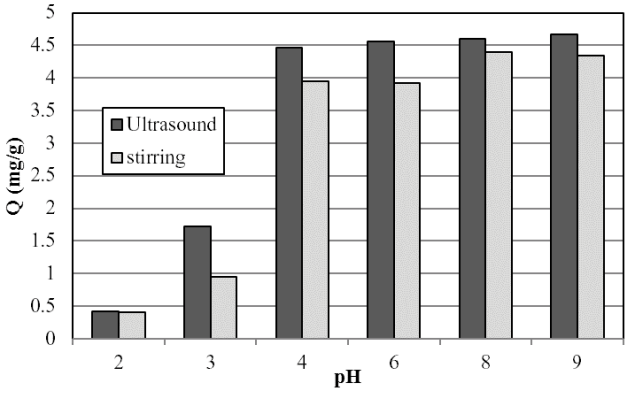

Fig. 11. Amount of malachite green biosorbed in the absence and presence of ultrasound for different initial solution pH (T = 21°C; biosorbent dose = 0.2 g/100 mL; initial concentration = 10 mg/L; stirring speed = 200 rpm or sonication power = 9 W).

$$\frac{t}{q_t} = \frac{1}{k_2 q_e^2} + \frac{1}{q_e} t \tag{5}$$

where k_2 is the pseudo-second-order rate constant (g/mg min), the initial biosorption rate (h, expressed in mg/g min) can be obtained when t approaches to zero.

$$h = k_2 q_e^2 \tag{6}$$

The values of k_2 and $q_{e,\text{cal}}$ were calculated from the intercepts ($1/k_2 q_e^2$) and slopes ($1/q_e$) of the plots of t/q_t vs. t, respectively.

The Elovich equation used for general application to chemisorption. The equation has been applied satisfactorily to some chemisorption processes and has been found to cover a wide range of slow adsorption rates. The same equation is often valid for systems in which the adsorbing surface is heterogeneous [47], and is formulated as:

$$q_t = \frac{1}{\beta}\ln(\alpha\beta) + \frac{1}{\beta}\ln(t) \tag{7}$$

where q_t is the biosorption capacity at time t (mg/g), α is the initial adsorption rate (mg/g min) and β is the desorption constant (g/mg). The values of α and β were calculated from the intercepts and slopes of the plots of q_t vs. ln(t).

The intra-particle diffusion model, based on the theory proposed by Weber and Morris, was used to identify the diffusion mechanism.

The kinetic data were analyzed using the Weber and Morris model which can be written as:

$$q_t = K_d t^{1/2} + C_d \tag{8}$$

where q_t is the adsorbed amount at any time, K_d is the intra-particle diffusion rate constant (mg/g min$^{1/2}$) and C_d is the intercept, which represents the thickness of the boundary layer. A larger intercept means a greater effect of the boundary layer [48].

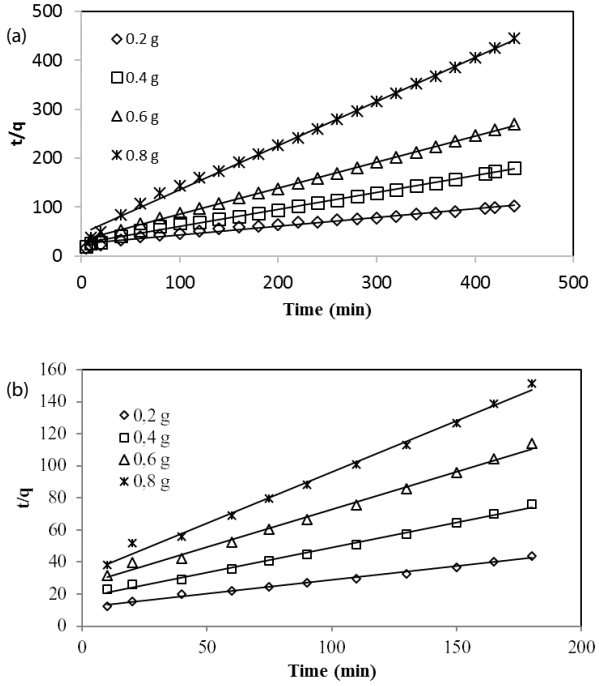

Fig. 12. Pseudo-second-order kinetics for the biosorption of MG by PLS (a) conventional method and (b) sonication method (conditions: 100 mL of MG solution; initial concentration = 10 mg/L; biosorbent mass = 0.2–0.8 g; acoustic power = 9 W; stirring speed = 200 rpm; temperature = 21°C).

The modeling of the experimental results of the sorption kinetics for different masses of sorbent by the Blanchard model for the conventional method (A) and sonication alone (B) is presented in Fig. 12. The parameters of the Blanchard model and the correlation coefficients for both methods are grouped in Table 2. Thus, the parameters of the Lagergren, Elovich and Weber and Morris models (Figures not shown) and their correlation coefficients are summarized in Table 2.

It can be seen that at all sorbent doses and for both methods, the linear regression correlation coefficient values were found to be higher ($r \geq 0.987$) and it has been shown that a good agreement between calculated q_e ($q_{e,\text{cal}}$) and experimental ($q_{e,\text{exp}}$). Consequently, the pseudo-second-order kinetics equation is adequate to describe the experimental data for the biosorption of MG on PLS for both methods. The coefficient "h" indicating the initial rate of sorption increased markedly when sonication was used instead of agitation. The higher mass transfer in the presence of ultrasonic irradiation seems to be a probable reason for this. Also, the coefficient "h" increased when the sorbent dose increased for both methods. This improvement may be explained by the greater accessibility of the biosorption sites with the highest biosorbent dose, resulting in an increase in the initial rate of adsorption.

After the Blanchard model, it is the Elovich model which is best suited especially for solutions under ultrasound where the correlation coefficients "r" are between 0.9912 and 0.9962 also for the agitated solutions the correlation coefficients "r" range from 0.9663 to 0.9957.

Table 2
Parameters of the kinetic models for the biosorption of MG on PLS at different sorbent dose

Model	Sorbent dose (g) "Stirring"				Sorbent dose (g) "Sonication"			
	0.2	0.4	0.6	0.8	0.2	0.4	0.6	0.8
Lagergren pseudo-first-order								
q_e (exp) (mg/g)	4.28	2.436	1.63	0.987	4.13	2.36	1.58	1.19
q_e (cal) (mg/g)	6.147	2.917	1.723	0.995	5.947	3.463	2.661	1.924
k_1 (min^{-1})	0.0105	0.0122	0.0120	0.0123	0.02830	0.03060	0.03450	0.03400
r	0.9354	0.9816	0.9898	0.9756	0.9748	0.9652	0.9458	0.9571
Blanchard pseudo-second-order								
k_2 (g/mg min)	0.0013	0.0048	0.0090	0.0181	0.0026	0.0054	0.0087	0.0125
q_e (cal) (mg/g)	5.549	2.866	1.871	1.107	5.811	3.210	2.120	1.568
h (mg/g min)	0.0401	0.0392	0.03156	0.02215	0.0869	0.0559	0.0389	0.0308
r	0.9873	0.9978	0.9997	0.9987	0.9965	0.9973	0.9966	0.9970
Elovich kinetics								
$\acute{\alpha}$ (mg/g min)	0.1275	0.10966	0.07731	0.06449	0.19668	0.12305	0.08481	0.06656
β (g/mg)	0.99612	1.79753	2.63852	4.80538	0.79064	1.39880	2.10881	2.84900
r	0.9663	0.9878	0.9957	0.9919	0.9912	0.9962	0.9944	0.9938
Intraparticle diffusion								
K_d (mg/g $min^{1/2}$)	0.2292	0.1606	0.1077	0.20060	0.37920	0.29470	0.20060	0.14680
C_d (mg/g)	–0.1719	–0.0745	0.02910	0.14680	–0.3897	–0.5114	–0.3453	–0.2275
r	0.9993	0.9978	0.9911	0.9958	0.9999	0.9982	0.9908	0.9876

The Elovich parameter "α" which represents the initial rate of sorption increases when the stirring is replaced by ultrasound, also, for both methods, this parameter increases when the dose of the sorbent increases.

Weber and Morris reported that if intraparticle diffusion is involved in the sorption process, by bringing the amount of MG adsorbed vs. $t^{1/2}$, we have to get a straight line. This step is the limiting step if the line passes through the origin.

The intercept provides information on the effect of the boundary layer, the larger it is, the greater the contribution of external diffusion in limiting the rate of sorption.

It emerges that the curves present several successive linearities, only the parameters of the first phase are indicated in Table 2. These parameters show that the lines of the linear regression have good correlation coefficients but do not pass through the origin ($C_d \neq 0$), which means that intraparticle diffusion is involved in the elimination mechanism, but is not the only limiting step.

3.11. Equilibrium isotherm studies

One of the main parameters required for designing an optimized system is the examination of the equilibrium isotherms for predicting the biosorption uptake of the biosorbent. The equilibrium data were fitted using four different isotherm models, namely the Langmuir (three linear forms), Freundlich, Temkin and Harkins–Jura models (Fig. 13).

The Langmuir model [49] assumes uniform energies of sorption onto the surface and no transmigration of sorbate in the plane of the surface. The Langmuir equation is given by the following relation:

$$\frac{q_e}{q_m} = \frac{bC_e}{1+bC_e} \tag{9}$$

where q_m is the maximum sorption capacity (mg/g) and b is the constant related to the free energy of sorption (L/mg).

The linearization of the Langmuir model is presented according to Stumm and Morgan [50] (Langmuir 1) as follows:

$$\frac{1}{q_e} = \frac{1}{q_m} + \frac{1}{bq_m} \times \frac{1}{C_e} \tag{10}$$

The linearization of the Langmuir model according to the representation of Weber [51] (Langmuir 2) is as follows:

$$\frac{C_e}{q_e} = \frac{1}{bq_m} + \frac{1}{q_m} \times C_e \tag{11}$$

The linearization of the model of Langmuir also appears according to the following form (Langmuir 3) [52]:

$$q_e = -\frac{1}{b}\frac{q_e}{C_e} + q_m \tag{12}$$

Freundlich isotherm is an empirical equation based on the sorption on a heterogeneous surface or surfaces supporting sites of various affinities [53]. The Freundlich equation can be written as:

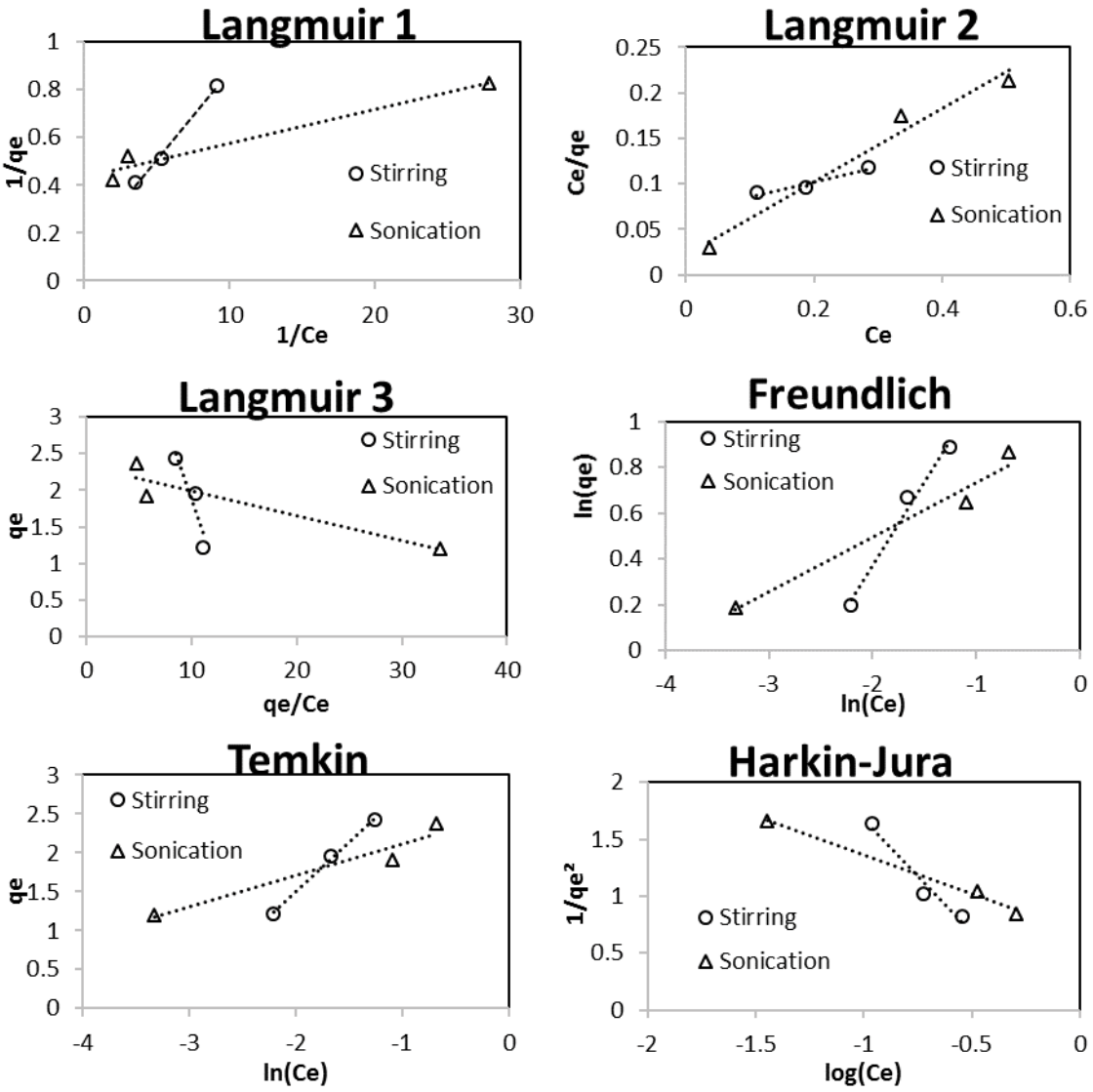

Fig. 13. Linear plots of isotherm models for the biosorption of MG on PLS: Langmuir (form 1, 2 and 3), Freundlich, Temkin and Harkins–Jura.

$$\ln q_e = \ln K_f + \frac{1}{n}\ln C_e \tag{13}$$

where K_f (mg$^{1-1/n}$/L$^{1/n}$ g) is Freundlich biosorbent capacity, $1/n$ is heterogeneity factor (if $n > 1$, the biosorption is a favorable physical process).

Temkin and Pyzhev [54] presented a model, which considered the interaction between sorbent and sorbate during biosorption. It was assumed that the heat of biosorption of all the molecules in the layer would decrease linearly with coverage due to sorbent-sorbate interaction [55]. Temkin equation can be depicted by:

$$q_e = \frac{R_g T}{b_t}\ln a_t + \frac{R_g T}{b_t}\ln C_e \tag{14}$$

where b_t is the Temkin constant related to the heat of adsorption (J/mol), a_t is the Temkin isotherm constant (L/mg), R_g is the ideal gas constant (8.314 J/mol K), and T is the absolute temperature (K).

The Harkins–Jura [56] adsorption isotherm can be expressed as:

$$\frac{1}{q_e^2} = \frac{B_{H-J}}{A_{H-J}} - \frac{1}{A_{H-J}}\log C_e \tag{15}$$

where A_{H-J} and B_{H-J} are Harkins–Jura constants.

The intercept and slope of each straight line were used to obtain the isotherm constants and given in Table 3. Referring to Fig. 13 as well as to Table 3, for stirring method, it was clear that Temkin model provided a very good fit (r = 0.9986) for the experimental equilibrium adsorption

data. It is concluded, according to Temkin's supposition, that the heat of biosorption of all molecules in the layer would decrease linearly with coverage due to the sorbent–sorbate interaction, and that the adsorption has a maximum energy distribution of uniform bonds. However, an exothermic process is possible due to the positive value of the b_t since b_t is associated the biosorptive heating [57]. Furthermore, it was found that the Temkin constant linked to the heat of biosorption was weak, approximately 2 kJ/mol (conventional method). The average binding energy value for the ion exchange mechanism, is 8–16 kJ/mol [58]. Owing to the low binding energy level of the investigated biosorbent, the interaction of the biosorbate with the biosorbent seems to be weak, depending on their degree of obeying to the Temkin model.

Based on the linear regression coefficient values, the most accurate model for stirred biosorption is the Temkin model, preceded by the form 1 of the Langmuir model and then the Freundlich model.

Additionally, the biosorption by means of sonication is best depicted by the Harkins–Jura model (r = 0.9956) followed by form 2 of the Langmuir model (r = 0.9858) and the Freundlich model (r = 0.9856). The experimental adsorption data fitting with the Harkins–Jura model confirms the occurrence of multilayer adsorption due to the heterogeneous pore distribution [57].

The most important characteristics of the Langmuir isotherm are given by the dimensionless Hall number (R_L) [59]:

$$R_L = \frac{1}{1 + bC_0} \tag{16}$$

where C_0: initial concentration of the solute (mg/L), b: Langmuir biosorption equilibrium constant (L/mg). If R_L = 0; the isotherm is irreversible, R_L between 0 and 1; the isotherm is favorable, R_L = 1; the isotherm is linear, R_L > 1; the isotherm is unfavorable.

In order to obtain the results of the evolution of the Hall parameter, which is measured from the three forms of the Langmuir equation, as a function of the initial concentration (for both methods), the following results are plotted in Fig. 14. These findings revealed that the R_L values ranged from 0 to 1, reflecting a favourable biosorption of MG onto the PLS.

In the case of the Freundlich model, the biosorption of MG is depicted by revealing heterogeneously spread biosorption sites on the PLS. To identify the biosorption, the value of n_F, called heterogeneity factor, was employed, whether it is linear (n_F = 1), chemical process (n_F < 1), and physical process (n_F > 1) [57]. Consequently, in this research, the biosorption process is physical and favourable with the n_F > 1.

Table 4 lists a comparison of adsorption capacity of the PLS with those obtained in the literature for the adsorption of MG. The calculated adsorption capacities exhibit a good capacity for dye adsorption from aqueous solutions. This result reveals that the PLS is effective adsorbent for MG dye removal from wastewater. It should be noted that

Table 3
Fitted isotherm models for MG biosorption on PLS at 21°C

Isotherm	Parameters	Stirring	Sonication
Langmuir (form 1)	q_m (mg/g)	7.18907261	2.29673863
	b (L/mg)	1.88227334	30.6619718
	r	0.99624294	0.97918333
Langmuir (form 2)	q_m (mg/g)	6.24219725	2.49438763
	b (L/mg)	2.2853067	18.1402715
	r	0.97066987	0.98584989
Langmuir (form 3)	q_m (mg/g)	6.0478	2.3234
	b (L/mg)	2.39406272	29.8507463
	r	0.9298387	0.93305948
Freundlich	K_f ($mg^{1-1/n}/L^{1/n}$ g)	6.22080923	2.65249313
	n	1.37741047	4.16666667
	r	0.99050492	0.985647
Temkin	a_t (L/mg)	24.1512242	531.209273
	b_t (J/mol)	1927.99811	6103.16105
	r	0.99864909	0.96778097
Harkins–Jura	A_{H-J} (mg^2/g^2)	0.50261359	1.45836372
	B_{H-J}	–0.15942903	0.98468718
	r	0.97703634	0.99559028

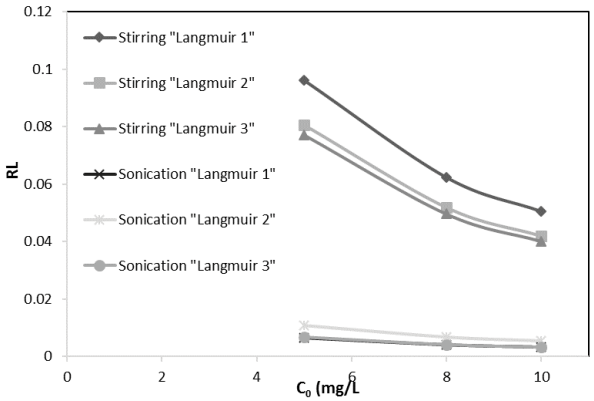

Fig. 14. Evolution of the Hall parameter, calculated from the three forms of the Langmuir equation, as a function of the initial concentration (for the stirring method and sonication method).

Table 4
Comparison of adsorption capacity of the PLS with that of various adsorbents

Adsorbent	q_m (mg/g)	Reference
Neem sawdust	4.35	[60]
Bentonite clay	7.716	[61]
Composite of coir pith activated carbon (CPAC)	4.4	[62]
CPAC/chitosan/SDS	4.8	[62]
Cellulose powder	2.422	[63]
Rice husk	7.40	[64]
Tamarind fruit shell	1.95	[65]
Untreated PLS	7.189	This work

the values and comparisons reported for MG dye removal capacity have only a relative meaning because of different testing conditions and methods.

4. Conclusion

The *Paracentrotus lividus* shells is a locally available, low-cost material and can be used as an alternative sorbent for the removal of MG or other cationic dyes from aqueous solutions without any chemical, heat, or other pretreatment.

The amount of MG biosorbed dropped as the dose of adsorbent was raised, the optimum sorbent dose was 0.4 g/100 mL. Minimum particle size showed greater biosorption than larger size for both methods. ultrasound has a similar effect to the increase in temperature; they accelerate the sorption process but the quantity sorbed at equilibrium remains invariant. When using ultrasound, the equilibrium time is reduced in half.

The amount of biosorbed dye rose with increasing shaking speed up to 200 rpm and initial solution pH. The ionic strength disfavors the sorption of dye. An increase in the initial dye concentration is associated with an increase in the biosorption ability of MG.

Kinetic data were adequately fitted by the pseudo-second-order model for both methods. For Equilibrium data of adsorption by stirring, the most suitable model is the Temkin model followed by form 1 of the Langmuir model followed by the Freundlich model. On the other hand, biosorption by sonication is better represented by the Harkins–Jura model followed by form 2 of the Langmuir model and the Freundlich model.

Therefore, the biosorbent is expected to be successfully utilized as a low-cost, alternative, eco-friendly, and effective sorbent for the removal of MG dye from aqueous solutions and the rate of biosorption increased markedly when sonication was used instead of agitation.

Acknowledgments

We are deeply in gratitude to the Ministry of Higher Education and Scientific Research of Algeria for its financial contribution (project n° A16N01UN410120210001).

References

[1] W. Stawiński, W. Agnieszka, O. Freitas, L. Chmielarz, G. Mordarski, S.A. Figueiredo, Simultaneous removal of dyes and metal cations using an acid, acid-base and base modified vermiculite as a sustainable and recyclable adsorbent, Sci. Total Environ., 576 (2017) 398–408.
[2] S. Karimifard, M. Reza, A. Moghaddam, Application of response surface methodology in physicochemical removal of dyes from waste water: a critical review, Sci. Total Environ., 640–641 (2018) 772–797.
[3] S. Attouti, B. Bestani, N. Benderdouche, L. Duclaux, Application of *Ulva lactuca* and *Systoceira stricta* algae-based activated carbons to hazardous cationic dyes removal from industrial effluents, Water Res., 47 (2013) 3375–3388.
[4] M. Essandoh, R.A. Garcia, Efficient removal of dyes from aqueous solutions using a novel hemoglobin/iron oxide composite, Chemosphere, 206 (2018) 502–512.
[5] A. Ansari, D. Nematollahi, A comprehensive study on the electrocatalytic degradation, electrochemical behavior and degradation mechanism of malachite green using electrodeposited nanostructured β-PbO_2 electrodes, Water Res., 144 (2018) 462–473.
[6] E. Forgacs, T. Cserhati, G. Oros, Removal of synthetic dyes from wastewaters: a review, Environ. Int., 30 (2004) 953–971.
[7] M.T. Yagub, T.K. Sen, S. Afroze, H.M. Ang, Dye and its removal from aqueous solution by adsorption: a review, Adv. Colloid Interface Sci., 209 (2014) 172–184.
[8] C.R. Holkar, A.J. Jadhav, D.V. Pinjari, N.M. Mahamuni, A.B. Pandit, A critical review on textile wastewater treatments: possible approaches, J. Environ. Manage., 182 (2016) 351–366.
[9] H. Hayat, Q. Mahmood, A. Pervez, Z.A. Bhatti, S.A. Baig, Comparative decolorization of dyes in textile wastewater using biological and chemical treatment, Sep. Purif. Technol., 154 (2015) 149–153.
[10] J. Mathieu-Denoncourt, C.J. Martyniuk, S.R. de Solla, V.K. Balakrishnan, V.S. Langlois, Sediment contaminated with the azo dye Disperse Yellow 7 alters cellular stress- and androgen-related transcription in *Silurana tropicalis* larvae, Environ. Sci. Technol., 48 (2014) 2952–2961.
[11] E.H. Koupaie, M.R.A. Moghaddam, S.H. Hashemi, Post-treatment of anaerobically degraded azo dye Acid Red 18 using aerobic moving bed biofilm process: enhanced removal of aromatic amines, J. Hazard. Mater., 195 (2011) 147–154.
[12] E. Alver, A.Ü. Metin, Anionic dye removal from aqueous solutions using modified zeolite: adsorption kinetics and isotherm studies, Chem. Eng. J., 200–202 (2012) 59–67.
[13] M. Monier, D.M. Ayad, Y. Wei, A.A. Sarhan, Adsorption of Cu(II), Co(II), and Ni(II) ions by modified magnetic chitosan chelating resin, J. Hazard. Mater., 177 (2010) 962–970.
[14] M. Ghaedi, F.N. Azad, K. Dashtian, S. Hajati, A. Goudarzi, M. Soylak, Central composite design and genetic algorithm applied for the optimization of ultrasonic-assisted removal of malachite green by ZnO nanorod-loaded activated carbon, Spectrochim. Acta, Part A, 167 (2016) 157–164.
[15] A. Asfaram, M. Ghaedi, K. Dashtian, G.R. Ghezelbash, Preparation and characterization of $Mn_{0.4}Zn_{0.6}Fe_2O_4$ nanoparticles supported on dead cells of Yarrowia lipolytica as a novel and efficient adsorbent/biosorbent composite for the removal of azo food dyes: central composite design optimization study, ACS Sustainable Chem. Eng., 6 (2018) 4549–4563.
[16] J.J.M. Órfão, A.I.M. Silva, J.C.V. Pereira, S.A. Barata, I.M. Fonseca, P.C.C. Faria, M.F.R. Pereira, Adsorption of a reactive dye on chemically modified activated carbons—influence of pH, J. Colloid Interface Sci., 296 (2006) 480–489.
[17] R. Malik, D. Ramteke, S. Wate, Adsorption of malachite green on groundnut shell waste based powdered activated carbon, Waste Manage., 27 (2007) 1129–1138.
[18] F. Kallel, F. Bouaziz, F. Chaari, L. Belghith, R. Ghorbel, S.E. Chaabouni, Interactive effect of garlic straw on the sorption and desorption of Direct Red 80 from aqueous solution, Process Saf. Environ. Prot., 102 (2016) 30–43.
[19] A. Bakka, M. Ait Taleb, N. Saffaj, A. Laknifli, R. Mamouni, A. Benlhachemi, B. Bakiz, Y. Diane, Patellidae shells waste as a biosorbent for the removal of aldrin pesticide from aqueous solutions, J. Eng. Sci. Technol., 13 (2018) 925–942.
[20] K. Aziz, F. Aziz, R. Mamouni, L. Aziz, N. Saffaj, Engineering of highly Brachychiton populneus shells@polyaniline biosorbent for efficient removal of pesticides from wastewater: optimization using BBD-RSM approach, J. Mol. Liq., 346 (2022) 117092, doi: 10.1016/j.molliq.2021.117092.
[21] Z. Li, X. Li, H. Xi, B. Hua, Effects of ultrasound on adsorption equilibrium of phenol on polymeric adsorption resin, Chem. Eng. J., 86 (2002) 375–379.
[22] M. Ghaedi, M.D. Ghazanfarkhani, S. Khodadoust, N. Sohrabi, M. Oftade, Acceleration of methylene blue adsorption onto activated carbon prepared from dross licorice by ultrasonic: equilibrium, kinetic and thermodynamic studies, J. Ind. Eng. Chem., 20 (2014) 2548–2560.
[23] B.S. Schueller, R.T. Yang, Ultrasound enhanced adsorption and desorption of phenol on activated carbon and polymeric resin, Ind. Eng. Chem. Res., 40 (2001) 4912–4918.

[24] D.D. Milenković, P.V. Dašić, V.B. Veljković, Ultrasound-assisted adsorption of copper(II) ions on hazelnut shell activated carbon, Ultrason. Sonochem., 16 (2009) 557–563.
[25] O. Hamdaoui, Removal of cadmium from aqueous medium under ultrasound assistance using olive leaves as sorbent, Chem. Eng. Process., 48 (2009) 1157–1166.
[26] O. Hamdaoui, Intensification of the sorption of Rhodamine B from aqueous phase by loquat seeds using ultrasound, Desalination, 271 (2011) 279–286.
[27] T.J. Mason, J.P. Lorimer, D.M. Bates, Quantifying sonochemistry: casting some light on a 'black art', Ultrasonics, 30 (1992) 40–42.
[28] E. Alipanahpour Dil, M. Ghaedi, A. Asfaram, A.A. Bazrafshan, Ultrasound wave assisted adsorption of Congo red using gold-magnetic nanocomposite loaded on activated carbon: optimization of process parameters, Ultrason. Sonochem., 46 (2018) 99–105.
[29] C. Djelloul, O. Hamdaoui, A. Alghyamah, S. Rezki, S. Mellouli, Combining ultrasound and stirring for the intensification of methylene blue biosorption from aqueous phase by jujube stone, Desal. Water Treat., 234 (2021) 277–287.
[30] D.D. Milenković, A.L. Bojić, V.B. Veljković, Ultrasound-assisted adsorption of 4-dodecylbenzene sulfonate from aqueous solutions by corn cob activated carbon, Ultrason. Sonochem., 20 (2013) 955–962.
[31] M. Roosta, M. Ghaedi, N. Shokri, A. Daneshfar, R. Sahraei, A. Asghari, Optimization of the combined ultrasonic assisted/ adsorption method for the removal of malachite green by gold nanoparticles loaded on activated carbon: experimental design, Spectrochim. Acta, Part A, 118 (2014) 55–65.
[32] A. Asfaram, M. Ghaedi, S. Hajati, A. Goudarzi, E.A. Dil, Screening and optimization of highly effective ultrasound-assisted simultaneous adsorption of cationic dyes onto Mn-doped Fe_3O_4-nanoparticle-loaded activated carbon, Ultrason. Sonochem., 34 (2017) 1–12.
[33] C. Djelloul, O. Hamdaoui, A. Alghyamah, Batch biosorption of the dye methylene blue from its aqueous solutions by Palm spathe: kinetic, isotherm, and thermodynamic studies, Desal. Water Treat., 231 (2021) 389–397.
[34] H. Ghodbane, E.K. Guechi, A. Alghyamah, O. Hamdaoui, Removal of malachite green from aqueous phase under ultrasound assistance using *Paracentrotus lividus* spines: equilibrium and kinetic studies, Desal. Water Treat., 210 (2021) 430–445.
[35] M. Aseel Aljeboree, A.N. Alshirifi, A.F. Alkaim, Kinetics and equilibrium study for the adsorption of textile dyes on coconut shell activated carbon, Arabian J. Chem., 10 (2017) S3381–S3393.
[36] E.K. Guechi, S. Benabdesselam, Removal of cadmium and copper from aqueous media by biosorption on cattail (*Typha angustifolia*) leaves: kinetic and isotherm studies, Desal. Water Treat., 173 (2020) 367–382.
[37] B.H. Hameed, A.A. Ahmad, Batch adsorption of methylene blue from aqueous solution by garlic peel, an agricultural waste biomass, J. Hazard. Mater., 164 (2009) 870–875.
[38] S. Cengiz, L. Cavas, Removal of methylene blue by invasive marine seaweed: Caulerpa racemosa var. cylindracea, Bioresour. Technol., 99 (2008) 2357–2363.
[39] O. Hamdaoui, E. Naffrechoux, L. Tifouti, C. Pétrier, Effects of ultrasound on adsorption–desorption of p-chlorophenol on granular activated carbon, Ultrason. Sonochem., 10 (2003) 109–114.
[40] E. Sharifpour, H.Z. Khafri, M. Ghaedi, A. Asfaram, R. Jannesar, Isotherms and kinetic study of ultrasound-assisted adsorption of malachite green and Pb^{2+} ions from aqueous samples by copper sulfide nanorods loaded on activated carbon: experimental design optimization, Ultrason. Sonochem., 40 (2018) 373–382.
[41] M. Gupta, H. Gupta, D.S. Kharat, Adsorption of Cu(II) by low cost adsorbents and the cost analysis, Environ. Technol. Innovation, 10 (2018) 91–101.
[42] S. Lagergren, About the theory of so-called adsorption of soluble substances, Kuling. Sven. Vetenskapsakad. Handl., 24 (1898) 1–39.
[43] G. Blanchard, M. Maunaye, G. Martin, Removal of heavy metals from waters by means of natural zeolites, Water Res., 18 (1984) 1501–1507.
[44] M.D. Low, Kinetics of chemisorption of gases on solids, Chem. Rev., 60 (1960) 267–312.
[45] W.J. Weber, J.C. Morris, Kinetics of adsorption on carbon from solutions, J. Sanit. Eng. Div., 89 (1963) 31–60.
[46] Y.S. Ho, G. McKay, The kinetics of sorption of basic dyes from aqueous solution by sphagnum moss peat, Can. J. Chem. Eng., 76 (1998) 822–827.
[47] M. Aseel Aljeboree, N. Abbas Alshirifi, F. Ayad Alkaim, Kinetics and equilibrium study for the adsorption of textile dyes on coconut shell activated carbon, Arabian J. Chem., 10 (2017) S3381–S3393.
[48] El.K. Guechi, O. Hamdaoui, Evaluation of potato peel as a novel adsorbent for the removal of Cu(II) from aqueous solutions: equilibrium, kinetic, and thermodynamic studies, Desal. Water Treat., 57 (2016) 10677–10688.
[49] I. Langmuir, The constitution and fundamental properties of solids and liquids, J. Am. Chem. Soc., 38 (1916) 2221–2295.
[50] W. Stumm, J.J. Morgan, Aquatic Chemistry, Weley-Interscience, 2nd ed., John Wiley and Sons, 1981.
[51] J. Weber Jr., Adsorption in Physicochemical Process for Water Quality Control, R.L. Metcalf, J.N. Pitts, Weley Interscience N.Y., 5 (1972) 199–259.
[52] O. Hamdaoui, E. Naffrechoux, Modeling of adsorption isotherms of phenol and chlorophenols onto granular activated carbon Part I. Two-parameter models and equations allowing determination of thermodynamic parameters, J. Hazard. Mater., 147 (2007) 381–394.
[53] H.M.F. Freundlich, Über die biosorption in lösungen, Z. Phys. Chem., 57 (1906) 385–470.
[54] M.J. Temkin, V. Pyzhev, Recent medications to Langmuir Isotherms, Acta Physiochim. USSR, 12 (1940) 217–222.
[55] I.A.W. Tan, J.C. Chan, B.H. Hameed, L.L.P. Lim, Biosorption behavior of cadmium ions onto phosphoric acid-impregnated microwave-induced mesoporous activated carbon, J. Water Process Eng., 14 (2016) 60–70.
[56] W.D. Harkins, E.J. Jura, The decrease (π) of free surface energy (γ) as a basis for the development of equations for adsorption isotherms; and the existence of two condensed phases in films on solids, J. Chem. Phys., 12 (1944) 112, doi: 10.1063/1.1723913.
[57] A.H. Karim, A.A. Jalil, S. Triwahyono, S.M. Sidik, N.H.N. Kamarudin, R. Jusoh, N.W.C. Jusoh, B.H. Hameed, Amino modified mesostructured silica nanoparticles for efficient adsorption of methylene blue, J. Colloid Interface Sci., 386 (2012) 307–314.
[58] Y.S. Ho, D.A. John Wase, C.F. Forster, Batch nickel removal from aqueous solution by sphagnum moss peat, Water Res., 29 (1995) 1327–1332.
[59] K.R. Hall, L.C. Eagleton, A. Acrivos, T. Vermeulen, Pore and solid diffusion kinetics in fixed-bed adsorption under constant pattern conditions, Ind. Eng. Chem. Fundam., 5 (1966) 212–223.
[60] S.D. Khattri, M.K. Singh, Removal of malachite green from dye wastewater using neem sawdust by adsorption, J. Hazard. Mater., 167 (2009) 1089–1094.
[61] S.S. Tahir, N. Rauf, Removal of a cationic dye from aqueous solutions by adsorption onto bentonite clay, Chemosphere, 63 (2006) 1842–1848.
[62] T.K. Arumugama, P. Krishnamoorthy, N.R. Rajagopalan, S. Nanthini, D. Vasudevan, Removal of malachite green from aqueous solutions using a modified chitosan composite, Int. J. Biol. Macromol., 128 (2019) 655–664.
[63] C.P. Sekhar, S. Kalidhasan, V. Rajesh, N. Rajesh, Biopolymer adsorbent for the removal of malachite green from aqueous solution, Chemosphere, 77 (2009) 842–847.
[64] S. Chowdhury, R. Mishra, P. Saha, P. Kushwaha, Adsorption thermodynamics, kinetics and isosteric heat of adsorption of malachite green onto chemically modified rice husk, Desalination, 265 (2011) 159–168.
[65] P. Saha, S. Chowdhury, S. Gupta, I. Kumar, R. Kumar, Assessment on the removal of malachite green using tamarind fruit shell as biosorbent, CLEAN – Soil Air Water, 38 (2010) 437–445.